Geophysical Research Letters

RESEARCH LETTER
10.1029/2020GL087468

Isobar Altitude Variations in the Upper Mesosphere Observed With IUVS-MAVEN in Response to Martian Dust Storms

L. Gkouvelis[1], J.-C. Gérard[1], F. González-Galindo[2], B. Hubert[1], and N. M. Schneider[3]

[1]LPAP, STAR Research institute, Université de Liège, Liège, Belgium, [2]Instituto de Astrofisica de Andalucía/CSIC, Granada, Spain, [3]LASP, University of Colorado, Boulder, CO, USA

Key Points:

- We present remote sensing observations of Martian upper atmospheric perturbations accompanying four dust storms
- We show the presence of a saturation of the 39 mPa isobar altitude rise near 0.3 infrared optical depth
- High temporal resolution observations of the initiation of the 2018 global dust storm indicate rapid response of the upper atmosphere

Correspondence to:
L. Gkouvelis,
l.gkouvelis@uliege.be

Citation:
Gkouvelis, L., Gérard, J.-C., González-Galindo, F., Hubert, B., & Schneider, N. M. (2020). Isobar altitude variations in the upper mesosphere observed with IUVS-MAVEN in response to Martian dust storms. *Geophysical Research Letters*, *46*, e2020GL087468. https://doi.org/10.1029/2020GL087468

Received 10 FEB 2020
Accepted 11 MAY 2020
Accepted article online 16 MAY 2020

Abstract We report limb measurements of the oxygen dayglow emission at 297.2 nm performed during four Martian dust storms. The emission peak provides a good remote sensing tool to probe changes of the altitude of the 39 mPa pressure level for the first time during dust storms. We illustrate the time variation of these changes and compare them with the infrared opacity in the lower atmosphere. We find that the 39 mPa level rises in response to the increase in dust opacity. It reaches a plateau, and additional dust load does not significantly increase its altitude. Numerical simulations with the LMD global circulation model shows a similar response, except for the event observed during MY33 regional storm when the model fails to reproduce the observed variations. Observations collected during the onset of the global dust storm in June 2018 show that the upper atmosphere rapidly responds within two Martian days to the increased amount of tropospheric dust.

Plain Language Summary Earlier studies have shown that the oxygen dayglow emission at 297.2 nm is a good tracer of the response of the upper atmosphere to atmospheric perturbations such as dust storms. In this work, we use MAVEN-IUVS observations during four different dust storm episodes in order to follow their influence on the atmospheric structure. We combine these measurements with concurrent observations of the dust load in the lower atmosphere monitored by infrared absorption. We find that the atmospheric layers move up as the atmospheric dust load increases. However, we show that there is a saturation effect limiting the rise of the layers at a given dust content. High time resolution observations performed during the first phase of the 2018 global dust storm indicate that the upper atmosphere responds quite fast following the onset of the storm.

1. Introduction

Martian dust storms are generally, but not always, observed during spring and summer in the southern hemisphere. Most are limited in size, atmospheric dust load, and opacity, sometimes reaching the regional or continental size. Occasionally, they cover most of the planetary surface and become global. These episodic events primarily affect the lower atmosphere, causing the surface to become unobservable in visible wavelengths for several weeks. However, evidence has accumulated that perturbations in the atmospheric density also occur at higher altitude, up to the exosphere. The time for dust settling near the south polar cap was estimated on the order of 60 days by Pang and Hord (1973).

The first indications that the Martian upper atmosphere responds to the dust load in the lower atmosphere were presented by Stewart and Hanson (1982). They analyzed Mariner 9 measurements of the altitude of the ionospheric peak following a major dust storm. They found that it was decreasing by 7.6 km over a time period of 60 days. This value was re-evaluated by Withers and Pratt (2013) who found a decay time of 10 km over a time interval of 18° of solar longitude (Ls), corresponding to 35 Earth days. They found that the atmospheric density had increased by more than an order of magnitude at the time of the first observations relative to dust-free periods. Keating et al. (1998) used measurements from the accelerometer on board the Mars Global Surveyor (MGS) spacecraft made during a regional storm. They reported a global response with an increase of ~8 km of the 1.26 nbar (130–140 km) pressure level at mid-latitudes during Martian year (MY)23. They observed a sharp rise and a decay time on the order of 90 days (Ls 227°–267°).

Withers and Pratt (2013) summarized the observed response of the upper atmosphere and ionosphere to dust storms, based on three different observational methods. They analyzed data collected by the MGS accelerometer, Mariner 9 and MGS radio occultation and SPICAM stellar occultation to determine the importance of the thermospheric perturbations generated in the upper atmospheric density. They showed that all three methods indicate that the density at a given altitude in the upper atmosphere increases following the onset of dust storms. These perturbations have been observed not only during the main dust season (Ls 180°–360°) but also earlier in the Martian year. They may reach an order of magnitude during major storms. The effects on the density extend over a wide range of latitudes. The rise time is on the order of a few days or less. The decay time can vary between 20° and 120° of Ls. The most likely explanation is the uplifting of the pressure levels follows a vertical temperature redistribution caused by dust aerosol heating and cooling in the lower atmosphere. This temperature perturbation, in turn, generates global dynamical effects. This scenario was confirmed by global circulation numerical simulations (Forget et al., 2009; Bell et al., 2007, González-Galindo et al. 2015; Bougher et al., 2017; Montabone & Forget, 2018). Recently, Fang et al. (2019) modeled the lifting up of the dayside ionosphere and showed that these perturbations propagate up to the magnetosphere and from the dayside to the nightside.

Earlier studies have demonstrated that the upper atmosphere responds on a large scale to the increased dust load of the lower atmosphere. Until recently, these measurements were made in situ based on local accelerometer, neutral, and electron density measurements. Only Jain et al. (2020) described the temperature perturbations associated with the 2018 global storm using IUVS limb observations.

In this study, we take advantage of the extensive coverage of dayglow observations performed with the Imaging Ultraviolet Spectrograph (IUVS) on board MAVEN during more than three Martian years. An earlier study (Gkouvelis et al., 2018) has shown that the peak altitude of dayglow emissions exhibits a marked seasonal variation (Gérard et al., 2019; Gkouvelis et al., 2020). The peak altitude of the oxygen 297.2 nm emission occurs at a fixed pressure level of P_0 of 39 $\pm$ 3 mPa. Here, we use observations of the airglow layer to remotely follow the altitude variations of this pressure level. We examine several examples of changes that occurred following regional or global dust storms, including the major global event of June 2018 (MY 34). We set limits on the time for the propagation of the disturbance into the upper atmosphere, and we examine the relation between the infrared dust opacity and the change of the mbar level. A better knowledge of these effects is important for current and future orbiting missions to Mars as they directly affect the atmospheric drag and thus the lifetime of low altitude orbiters.

2. Methodology

We now describe the IUVS data set used in this study and the procedure applied for the data analysis of the oxygen dayglow emission at 297.2 nm data analysis.

2.1. IUVS Observations

During the periods of observations described in this study, MAVEN was on an elliptical orbit with a 6,000 km apoapsis and a periapsis ~160 km (Jakosky et al., 2015). Near periapsis, the IUVS spectral imager (McClintock et al., 2015) observes the planetary limb between 115 and 340 nm in two separate (MUV and FUV) spectral channels. The FUV channel includes the OI emission at 297.2 nm. The spectral resolution of the FUV channel is ~0.6 nm. The instrument is equipped with a pivoting mirror that was scanning across the limb. The size of the entrance slit is 11.3° × 0.06°. The IUVS array detectors record images that contain spatial information in one and spectral information in the other dimension. In the limb observing mode, the entrance slit is parallel to the orbital plane and to the direction of the spacecraft motion. The mirror reflects the light entering to slit onto the detectors before it rotates to observe a different tangent point altitude to progressively build up an emission limb profile. Up to 12 individual limb scans are acquired per orbit over the period of 22 min of the limb observations. In this study, we use level 1C processed data in version 13, available on NASA's PDS archives. The processed data provide calibrated brightness of individual emissions. They are obtained based on a multiple linear regression (MLR) method. The various spectral components (lines or molecular bands) of each spectrum are fitted with synthetic spectra following convolution with the instrumental line spread function, taking into account the reflected solar background (Jain et al., 2015; Stevens et al., 2015).

The contribution of scattered solar light is found to be negligible for tangent altitudes above ~100 km. Below this altitude, Rayleigh scattering progressively increases. The quality of the background removal at 297.2 nm using this method was demonstrated by Gkouvelis et al. (2018).

2.2. Measurements of the 297.2 nm Dayglow Emission

The method to describe the seasonal variations of the isobar was described by Gkouvelis et al. (2020). It is based on the specificity that the O(^{1}S) level is solely excited by photodissociation of CO_2 by solar Lyman radiation. Since CO_2 is by far the dominant constituent below the homopause, the excitation conditions of the O(^{1}S) atoms are close to those producing Chapman layers. The altitude of the emission of the lower 297.2 nm peak is therefore controlled by the overlying CO_2 column density (Gkouvelis et al., 2018). Numerical simulations have indicated that the airglow peak altitude varies in such a way that it is located at the altitude where the overhead CO_2 column density is equal to 2.1×10^{19} cm^{-2}, corresponding to a pressure P_0 of 39 mPa. In this study, we do not average data collected over different orbits in order to reach optimal time and latitudinal resolution. Instead, we construct limb profiles by grouping no more than three or four consecutive IUVS limb scans. This averaging typically corresponds to a time interval of several minutes and covers less than 10 degrees of latitude. The standard deviation of the altitudes within a group of limb scans does not exceed 2.5 km. The IUVS limb data were collected during daytime (solar zenith angle <75°) between MAVEN first science orbits in October 2014 and August 2018 when the spacecraft altitude was near periapsis at an altitude less than 400 km. The spatial and temporal coverage was limited by the MAVEN orbital configuration and operational constraints. Since the column density, and thus the pressure level, varies with the solar zenith angle (SZA) θ by a factor close to $\cos(\theta)$ for $\theta < 80°$, we can calculate the altitude of the isobar level from the relation $Z_{max} \nearrow \ln[1/\cos(\theta)]$ as was shown in Gkouvelis et al. (2020).

3. Results

3.1. Time Evolution

We focus on four time intervals when dust storms occurred during IUVS observations and satisfying the conditions defined in section 2. They cover the periods 18 October to 1 December 2014 (MY32), 7 March to 2 June 2015 (MY32), 5 October 2016 to 2 January 2017 (MY33), and 1 June to 14 2018 (MY34). The last one obscured a large fraction of the Martian disk and is the only global dust storm observed since the beginning of the MAVEN mission. Its onset and development have been described by Sánchez-Lavega et al. (2019), Kass et al. (2020), and Elrod et al. (2020). It started on 30 May 2018 (Ls = 185°) in the northern hemisphere in Acidalia Planitia (32°N) and rapidly extended southward, eastward, and westward. On 9 June, it covered an estimated area of about 2.5×10^7 km^2, and maximal visible opacity reached values as high as 70 km.

The right hand side panels of Figure 1 show the four samples of IUVS observations of the peak altitude of the lower peak of the OI 297.2 nm dayglow collected during time period when the storm was in an evolutionary phase in terms of dust load. The evolution of the dust opacity for these specific time periods and spatial regions is presented on the left hand panels. These panels show gridded maps of dust column opacity near 9.3 μm normalized to the reference pressure level of 610 Pa that have been built by Montabone et al. (2015) and Montabone et al. (2020) for MY34, based on infrared observations from Mars orbiting satellites. We use these data in digital format with a bin size of 6° of solar longitude by 5° of latitude for comparison with the IUVS data. The P_0 isobar altitude is plotted on a color scale ranging from 75 to 95 km. Each pixel represents an average of at least three vertical scans of nearby observations in terms of time and latitude. A few characteristics may be derived from this comparison:

1. The time period spanned by the IUVS observations during the MY34 global storm is much shorter than the other three events (8° of Ls compared to 28° to 50° for the other events). It covers the onset phase of the storm and its subsequent southward propagation.
2. A connection between the onset of the opacity increase and the upward shift of the altitude of the reference level P_0 during the development phase of the storms is clearly apparent. It is most conspicuous after Ls = 265° during MY33 at high southern latitudes and Ls = 189° during MY34 at high southern latitudes. We also note the occurrence of relatively high peak altitudes between 0 and 10°N as early as Ls <220°, before the occurrence of the maximum dust opacity.

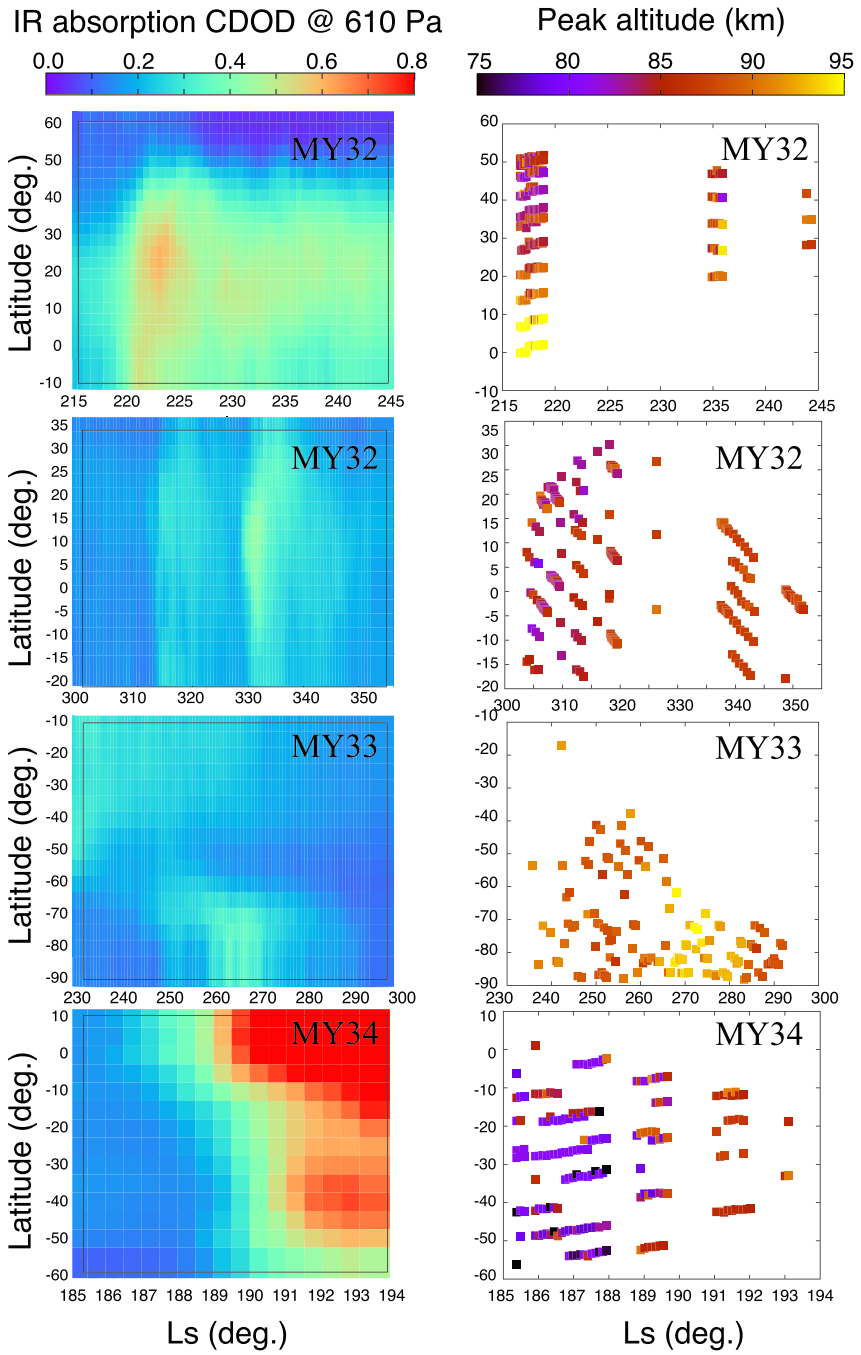

Figure 1. Comparison between the observed 297.2 nm peak altitude evolution with the corresponding dust opacity observations. The left column illustrates the infrared dust column opacity at 610 Pa, and the right column shows the changing peak altitude of the OI 297.2 nm emission.

3. The highest dust load was observed during the June 2018 global (MY34) dust storm in southern low latitudes region where it reached values as high as 0.63. This is higher than during the MY33 sequence when the highest opacity was limited to ~0.4. However, we note that the P_0 altitude remained close to 80 km, while it moved up to 95 km during the MY 33 storm.
4. The MY34 global storm development started at fall equinox (Ls = 185°), earlier than the other cases which were observed during northern winter. This seasonal difference explains why the pre-storm altitude of the 610 Pa level was lower by as much as 20 km. The study of the seasonal variation of the

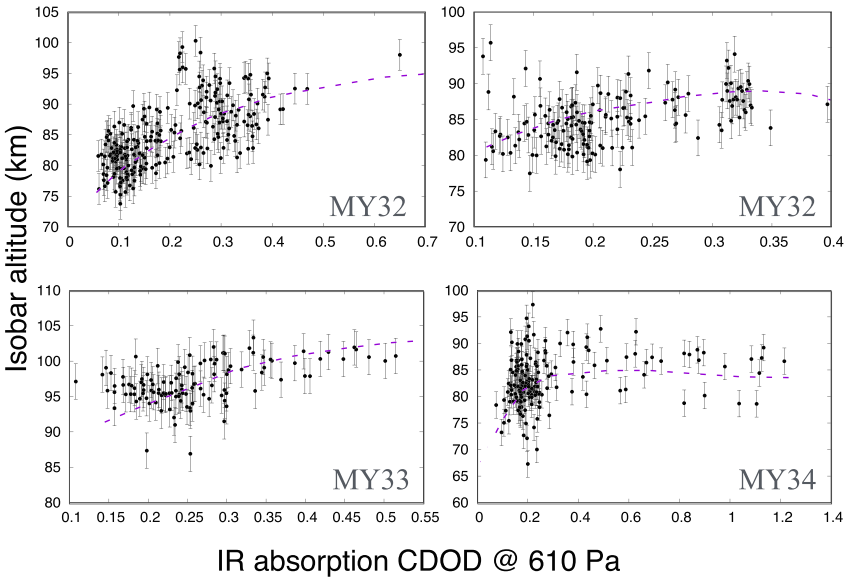

Figure 2. Variation of the 39 mPa pressure level during the four dust storms versus the infrared opacity at the same location and time. The dashed line represents a second-order least squares fit to the observations.

altitude of the OI 297.2 nm dayglow showed that the altitude typically rises from about 80 km up to more than 90 km between Ls = 185° and 270° (Gkouvelis et al., 2020).

3.2. Relation Between the Dust Load and the Isobar Altitude

We now compare pixel-by-pixel the isobar altitude with the corresponding dust load measurements. Figure 2 illustrates the dependence of the peak altitude with the atmospheric dust load for the different cases. The peak altitudes vary from less than 75 km up to about 100 km. However, the altitude associated with the period of low opacity varies in each case. First, the maximum level of opacity occurred during the MY34 observations. Second, it clearly shows a non-linear increase of the isobar altitude as the opacity varies from low values up to approximately 0.3. These differences correspond to different seasons so that the peak altitude of the emission is different even in the absence of dust activity. Third, it reveals an interesting feature: In all four cases, the peak altitude reaches a plateau. This is particularly obvious during the MY34 global storm.

A more detailed description of the relation observed during the MY34 storm is shown in Figure 3 where the altitude of the 39 mPa level and the dust opacity have been plotted together. For this comparison, each individual IUVS altitude observation is compared with the infrared opacity measurement at the same location extracted from the daily map (every Sol) from Montabone et al. (2020). The time difference between two corresponding data points is therefore at most 0.5 sol. Both samples follow the same pattern in time, indicating that the dust load in the lower atmosphere can perturbate almost instantly the upper atmosphere. To quantify this result we have correlated the samples. The linear correlation coefficient is 0.58 for a sample of 98 values. Applying the Fisher transformation, the test indicates that correlation is validated at a confidence level of over 99%. The rise time during the MY33 regional storm was on the order of a 3° of Ls, that is, about five Earth days. The decay is somewhat slower with a characteristic time of eight to 10 Earth days. At the time resolution of the measurements and considering the altitude uncertainties, there is no indication of a significant time lag (less than 0.1° of LS or 2 sols) between the changes in dust load and the isobar altitude.

4. Model Simulations

As mentioned in section 1, the most likely explanation of the changing altitude following a dust storm is an increase of the CO_2 density generated by perturbations of the vertical temperature distribution. Model simulations have demonstrated that density perturbations mostly result from changes in the temperature vertical structure generated by the increased opacity during dust storms. We use the model of the Laboratoire de

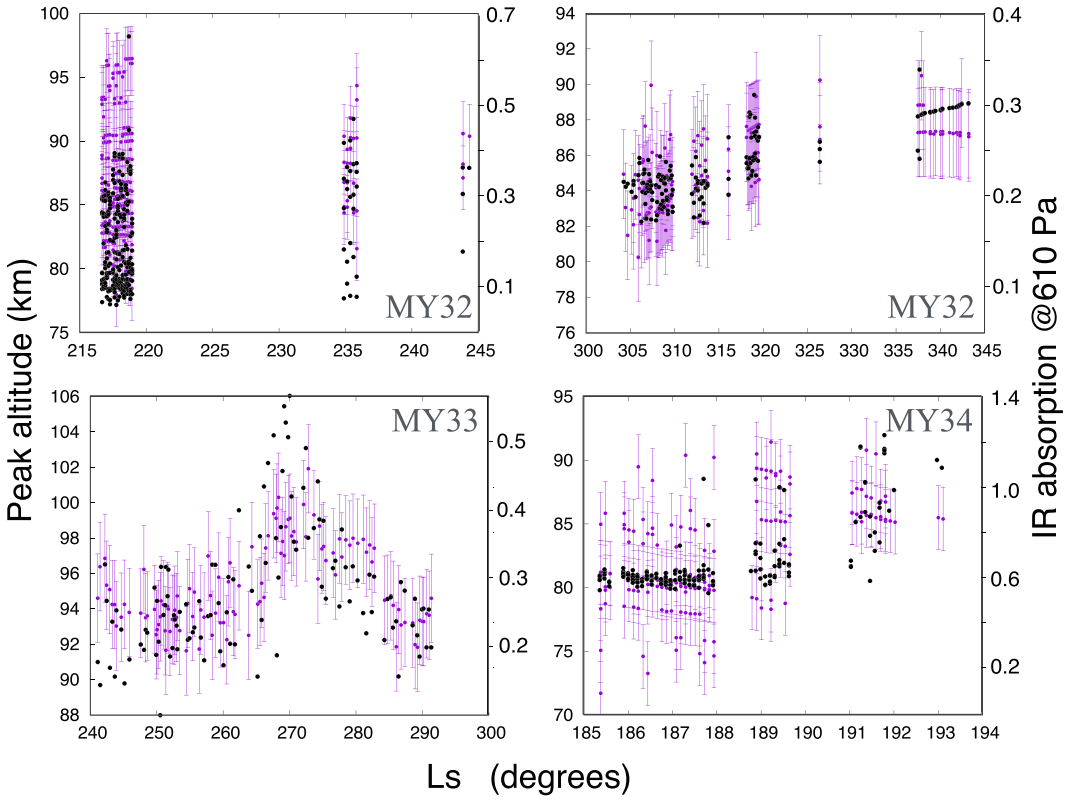

Figure 3. Simultaneous time variation of the altitude of the 39 mPa level and infrared dust opacity at 610 Pa measured during the four different Martian dust storms. The purple dots indicate the 297.2 nm peak altitude derived from the IUVS observations, and their uncertainty bars and the black dots correspond to the observed infrared dust opacity.

Météorologie Dynamique (LMD) to compare numerical simulations of the altitude of the 39 mPa level with our four sets of observations described in section 3. The extension of the LMD model (Forget et al., 1999) up to the thermosphere used in this study was described by González-Galindo et al. (2015). In brief, it includes processes at the surface and radiative processes including the role of CO_2 and dust in the lower atmosphere, and absorption of solar ultraviolet radiation by CO_2, O_2, OH_2, H_2O, and H_2O_2. Non-LTE effects are taken into account and heating and cooling by CO_2 are parameterized. Thermal conduction, molecular diffusion of minor constituents, and chemical reactions are also included. The model calculations are carried out using the same conditions of solar longitude, latitude, and solar activity as the observations. The LMD simulations are driven by the IR opacity measurements shown in Figure 1.

The results of the comparison are shown in Figure 4. The LMD simulations are in satisfactory agreement for MY32, except for the data collected around Ls = 235° when the modeled altitude exceed the observations by about 7 km. The MY32 comparison indicates that the simulated altitude is on the high side of the observations for Ls < 320° and on the high side for Ls > 337°. Some disagreement between the IUVS observations and the LMD model is observed during the MY33 time sequence. Figure 5 shows the predicted time evolution of the altitude of the 39 mPa pressure level at 80°S over a longer time frame after Ls = 180°. It shows a sharp rise that could not be observed by IUVS, followed by a slow continuous decrease that is also seen in the peak altitude of the 297.2 nm emission. The model does not anticipate the altitude rise near Ls = 265°, but IUVS also observes the altitude drop after Ls = 270°. This altitude rise is however limited compared to the altitude change predicted by the LMD model during the full period of this regional dust storm.

The calculated altitude is in quite good agreement for MY34 when both observations and simulations show the response to the increasing dust load after Ls = 188°. The model does not correctly predict the altitude rise observed for Ls > 265° during Martian year 33 when the altitude rapidly increased by about 7 km. Actually,

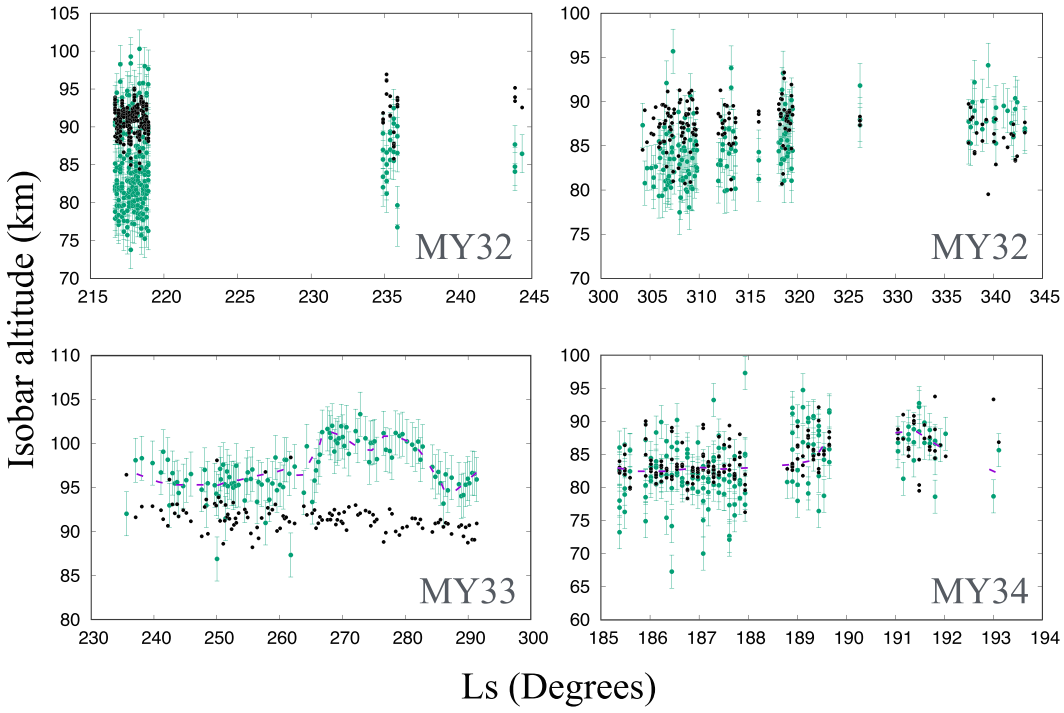

Figure 4. Comparisons between IUVS observations (green dots) and LMD simulations (black dots) for the same conditions are shown for four different periods of dust load activity described in Figure 1. A smoothed red dashed line has been added for MY33 and MY34, two cases when the time coverage is nearly continuous.

the LMD evolution is a slow decreasing trend of the isobar altitude. This is the most dramatic data model discrepancy observed among the four cases.

Figure 1 indicates that this rise was mostly observed between 90°S and 60°S, in contrast to MY34 when all southern latitudes exhibited the altitude variation. The cause of this discrepancy is not known, but it is probably a consequence of an underestimate of the atmospheric temperature during this event.

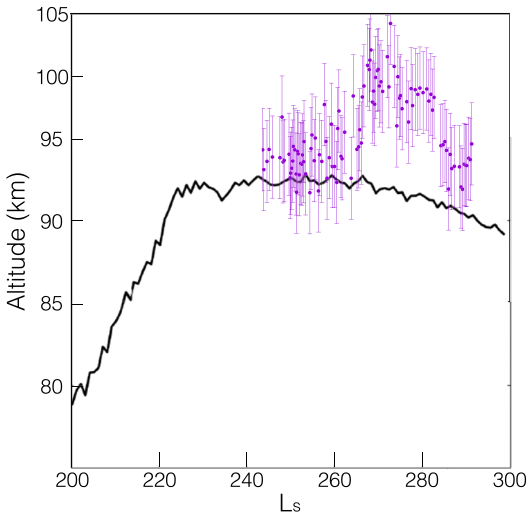

Figure 5. Martian year 33 case, covering a wider LS range of the LMD curve. The LMD predicts the rise in the altitude of the isobar due to the dust storm except a fast peak between Ls = 270° and 278° that it was observed from IUVS.

5. Conclusions and Summary

Observations of the altitude of the OI 297.2 nm emission peak during four dust storms observed that occurred in Martian years 32 to 34 indicate the following

- The altitude of the emission peak and the 39 mPa pressure level varies during periods of increased infrared opacity in response to perturbations of atmospheric temperature and density.
- This level moves by up to 20 km when the dust load increases in the lower atmosphere and decreases when the storm decays. The parallel time evolution of the two curves indicates that the correlation is statistically significant for the MY33 storm.
- A plateau in this uplift is observed when the infrared opacity at 610 Pa exceeds 0.35, suggesting a saturation effect in the dust heating owing to the evolving dust load, resulting in a leveling off of temperature and the subsequent density perturbation at the given 39 mPa pressure level.
- These results are in agreement with earlier observations by other techniques (atmospheric drag, mass spectrometer, and electron

density vertical distribution) of the perturbations in the thermosphere and the upward displacement of the ionospheric density peak during dust storms.

- Comparisons with simulations with the LMD general circulation model indicate that a general agreement is obtained with the IUVS observations. However, during the MY33 storm, the LMD model predicts altitudes lower than observed, a slow decrease during the storm period in contrast to the observed sharp rise.

Data Availability Statement

The IUVS-MAVEN data sets were obtained from NASA's Planetary Data System (PDS) available online (http://atmos.nmsu.edu/data_and_services/atmospheres_data/MAVEN/maven_main.html).

Acknowledgments

B. Hubert is a research associate of the Belgian Fund for Scientific Research (FNRS). F.G.G. is funded by the Spanish Ministerio de Ciencia, Innovación y Universidades, the Agencia Estatal de Investigacion and EC FEDER funds under project RTI2018-100920-J-I00, and acknowledges financial support from the State Agency for Research of the Spanish MCIU through the "Center of Excellence Severo Ochoa" award to the Instituto de Astrofísica de Andalucía (SEV-2017-0709). We acknowledge L. Montabone for providing infrared opacity data before their final publication. This project acknowledges funding by the Belgian Science Policy Office (BELSPO), with the financial and contractual coordination by the ESA Prodex Office. IUVS archive, V13 was used for this study. This work utilized the RMACC Summit supercomputer, which is supported by the National Science Foundation (awards ACI-341 1532235 and ACI-1532236), the University of Colorado Boulder, and Colorado State University. The Summit supercomputer is a joint effort of the University of Colorado Boulder and Colorado State University.

References

Bell, J. M., Bougher, S. W., & Murphy, J. R. (2007). Vertical dust mixing and the interannual variations in the Mars thermosphere. *Journal of Geophysical Research*, *112*, E12002. https://doi.org/10.1029/2006JE002856

Bougher, S. W., Roeten, K. J., Olsen, K., Mahaffy, P. R., Benna, M., Elrod, M., Jain, S. K., Schneider, N. M., Deighan, J., Thiemann, E., Eparvier, F. G., Stiepen, A., & Jakosky, B. M. (2017). The structure and variability of Mars dayside thermosphere from MAVEN NGIMS and IUVS measurements: Seasonal and solar activity trends in scale heights and temperatures. *Journal of Geophysical Research: Space Physics*, *122*, 1296–1313. https://doi.org/10.1002/2016JA023454

Elrod, M. K., Bougher, S. W., Roeten, K., Sharrar, R., & Murphy, J. (2020). Structural and compositional changes in the upper atmosphere related to the PEDE-2018 dust event on Mars as observed by MAVEN NGIMS. *Geophysical Research Letters*, *47*, https://doi.org/10.1029/2019GL084378

Fang, X., Pawlowski, D., Ma, Y., Bougher, S., Thiemann, E., Eparvier, F., et al. (2019). Mars Upper Atmospheric Responses to the 10 September 2017 Solar Flare: A Global, Time-Dependent Simulation. *Geophysical Research Letters*, *46*(16), 9334–9343. https://doi.org/10.1029/2019gl084515

Forget, F., Hourdin, F., Fournier, R., Hourdin, C., Talagrand, O., Collins, M., et al. (1999). Improved general circulation models of the Martian atmosphere from the surface to above 80 km. *Journal of Geophysical Research*, *104*(E10), 24,155–24,175. https://doi.org/10.1029/1999JE001025

Forget, F., Montmessin, F., Bertaux, J. L., González-Galindo, F., Lebonnois, S., Quemerais, E., Reberac, A., Dimarellis, E., & López-Valverde, M. A. (2009). Density and temperatures of the upper Martian atmosphere measured by stellar occultations with Mars express SPICAM. *Journal of Geophysical Research*, *114*, E01004. https://doi.org/10.1029/2008JE003086

Gérard, J. C., Gkouvelis, L., Ritter, B., Hubert, B., Jain, S. K., & Schneider, N. M. (2019). MAVEN-IUVS observations of the CO_2^+ UV doublet and CO Cameron bands in the Martian thermosphere: Aeronomy, seasonal, and latitudinal distribution. *Journal of Geophysical Research: Space Physics*, *124*, 5816–5827. https://doi.org/10.1029/2019JA026596

Gkouvelis, L., Gérard, J. C., Ritter, B., Hubert, B., Schneider, N. M., & Jain, S. K. (2018). The O(1S) 297.2-nm dayglow emission: A tracer of CO_2 density in the Martian lower thermosphere. *Journal of Geophysical Research: Planets*, *123*, 3119–3132. https://doi.org/10.1029/2018JE005709

Gkouvelis, L., Gérard, J. C., Ritter, B., Hubert, B., Schneider, N. M., & Jain, S. K. (2020). Airglow remote sensing of the seasonal variation of the Martian upper atmosphere: Four years of MAVEN limb observations. *Icarus*, *341*, 113666. https://doi.org/10.1016/j.icarus.2020.113666

González-Galindo, F., López-Valverde, M. A., Forget, F., García-Comas, M., Millour, E., & Montabone, L. (2015). Variability of the Martian thermosphere during eight Martian years as simulated by a ground-to-exosphere global circulation model. *Journal of Geophysical Research: Planets*, *120*, 2020–2035. https://doi.org/10.1002/2015JE004925

Jain, S. K., Bougher, S. W., Deighan, J., Schneider, N. M., González Galindo, F., Stewart, A. I. F., et al. (2020). Martian thermospheric warming associated with the planet encircling dust event of 2018. *Geophysical Research Letters*, *47*, https://doi.org/10.1029/2019GL085302

Jain, S. K., Stewart, A. I. F., Schneider, N. M., Deighan, J., Stiepen, A., Evans, J. S., Stevens, M. H., Chaffin, M. S., McClintock, W. E., Clarke, J. T., Holsclaw, G. M., Lo, D. Y., Lefévre, F., Montmessin, F., Thiemann, E. M. B., Crismani, M., Eparvier, F., & Jakosky, B. M. (2015). The structure and variability of Mars upper atmosphere as seen in MAVEN/IUVS dayglow observations. *Geophysical Research Letters*, *42*, 9023–9030. https://doi.org/10.1002/2015GL065419

Jakosky, B. M., Lin, R. P., Grebowsky, J. M., Luhmann, J. G., Mitchell, D. F., Beutelschies, G.,Priser, T., Acuna, M., Andersson, L., Baird, D., Baker, D., Bartlett, R., Benna, M, Bougher, S., Brain, D., Cauffman, S., Chamberlin, P., Chaufray, J.-Y., Cheatom, O., Clarke, J., Connerney, J., Cravens, T., Curtis, D., Delory, G., Demcak, S., DeWolfe, A., Eparvier, F., Ergun, R., Eriksson, A., Espley, J., Fang, X., Folta, D., Fox, J., Gomez-Rosa, C., Habenicht, S, Halekas, J., Holsclaw, G., Houghton, M., Howard, R., Jarosz, M., Jedrich, N., Johnson, M., Kasprzak, W., Kelley, M., King, T., Lankton, M., Larson, D., Leblanc, F., Lefevre, F., Lillis, R., Mahaffy, P., Mazelle, C., McClintock, W., McFadden, J., Mitchell, D. L., Montmessin, F., Morrissey, J., Peterson, W., Possel, W., Sauvaud, J.-A., Schneider, N., Sidney, W., Sparacino, S., Stewart, A. I. F., Tolson, R., Toublanc, D., Waters, C., Woods, T., Yelle, R., & Zurek, R. (2015). The Mars atmosphere and volatile evolution (MAVEN) mission. *Space Science Reviews*, *195*(1–4), 3–48. https://doi.org/10.1007/s11214-015-0139-x

Kass, D. M., Schofield, J. T., Kleinböhl, A., McCleese, D. J., Heavens, N. G., Shirley, J. H., & Steele, L. J. (2020). Mars climate sounder observation of Mars' 2018 global dust event. *Geophysical Research Letters*, *47*, 2019GL083931. https://doi.org/10.1029/2019GL083931

Keating, G. M., Bougher, S. W., Zurek, R. W., Tolson, R. H., Cancro, G. J., Noll, S. N., , Parker, J. S., Schellenberg, T. J., Shane, R. W., Wilkerson, B. L., Murphy, J. R., Hollingsworth, R. M., Joshi, M., Pearl, S., Bougher, J. C., Conrath, B. J., Smith, M. D., Clancy, R. T., Blanchard, R. C., Wilmoth, R. G., Rault, D. F., Martin, T. Z., Lyons, D. T., Esposito, P. B., Johnston, M. D., Whetzel, C. W., Justus, C. G., & Babicke, J. M. (1998). The structure of the upper atmosphere of Mars: In situ accelerometer measurements from Mars global surveyor. *Science*, *279*(5357), 1672–1676. https://doi.org/10.1126/science.279.5357.1672

McClintock, W. E., Schneider, N. M., Holsclaw, G. M., Clarke, J. T., Hoskins, A. C., Stewart, I., et al. (2015). The imaging ultraviolet spectrograph (IUVS) for the MAVEN mission. *Space Science Reviews*, *195*(1–4), 75–124. https://doi.org/10.1007/s11214-014-0098-7

Montabone, L., & Forget, F. (2018). Forecasting dust storms on Mars: A short review. In J. S. Levine, D. Winterhalter, & R. L. Kerschmann (Eds.), *Dust in the atmosphere of Mars and its impact on human exploration* (Chap. 8, Vol. 1966, pp. 132–151). UK: Cambridge scholars publishing. https://www.cambridgescholars.com/download/sample/64708

Montabone, L., Forget, F., Millour, E., Wilson, R. J., Lewis, S. R., Cantor, B., et al. (2015). Eight-year climatology of dust optical depth on Mars. *Icarus*, *251*, 65–95. https://doi.org/10.1016/j.icarus.2014.12.034

Montabone, L., Spiga A., Kass D. M., Kleinböhl A., Forget F., Millour E. (2020). Martian Year 34 Column Dust Climatology from Mars Climate Sounder Observations: Reconstructed Maps and Model Simulations. *Journal of Geophysical Research: Planets*. https://doi.org/10.1029/2019je006111

Pang, K., & Hord, C. W. (1973). Mariner 9 ultraviolet spectrometer experiment: 1971 Mars' dust storm. *Icarus*, *18*(3), 481–488. https://doi.org/10.1016/0019-1035(73)90157-7

Sánchez-Lavega, A., del Río-Gaztelurrutia, T., Hernández-Bernal, J., & Delcroix, M. (2019). The onset and growth of the 2018 Martian global dust storm. *Geophysical Research Letters*, *46*, 6101–6108. https://doi.org/10.1029/2019GL083207

Stevens, M. H., Evans, J. S., Schneider, N. M., Stewart, A. I. F., Deighan, J., Jain, S. K., Crismani, M., Stiepen, A., Chaffin, M. S., McClintock, W. E., Murphy, J. R., Hollingsworth, R. M., Holsclaw, G. M., Lefévre, F., Lo, D. Y., Conrath, B. J., Clarke, J. T., Montmessin, F., Bougher, S. W., & Jakosky, B. M. (2015). New observations of molecular nitrogen in the Martian upper atmosphere by IUVS on MAVEN. *Geophysical Research Letters*, *42*, 9050–9056. https://doi.org/10.1002/2015GL065319

Stewart, A. J., & Hanson, W. B. (1982). Mars' upper atmosphere—Mean and variations. *Advances in Space Research*, *2*(2), 87–101. https://doi.org/10.1016/0273-1177(82)90109-0

Withers, P., & Pratt, R. (2013). An observational study of the response of the upper atmosphere of Mars to lower atmospheric dust storms. *Icarus*, *225*(1), 378–389. https://doi.org/10.1016/j.icarus.2013.02.032